ChemPhysChem

Research Article
doi.org/10.1002/cphc.202300271

Chemistry Europe
European Chemical Societies Publishing

www.chemphyschem.org

Elucidating the Effect of Ion Exchange Protocol on the Copper Exchange Efficacy, Copper Siting, and SCR activity in Cu-SSZ-13

Aibolat Koishybay,[a] Charles Umhey,[b] Chun-Te Kuo,[c] Kyle Groden,[b] Jean-Sabin McEwen,[b, d, e, f, g] Ayman M. Karim,[c] and Daniel F. Shantz*[a]

The influence of the copper ion exchange protocol on SCR activity of SSZ-13 is quantified. Using the same parent SSZ-13 zeolite, four exchange protocols are used to assess how exchange protocol impacts metal uptake and SCR activity. Large differences in the SCR activity, nearly 30 percentage points at 160 °C at constant copper content, are observed for different exchange protocols implying that different exchange protocols lead to different copper species. Hydrogen temperature programmed reduction on selected samples and infrared spectroscopy of CO binding corroborates this conclusion as the reactivity at 160 °C correlates with the intensity of the IR band at 2162 cm^{-1}. DFT-based calculations show that such an IR assignment is consistent with CO adsorbed on a Cu(I) cation within an eight-membered ring. This work shows that SCR activity can be influenced by the ion exchange process even when different protocols lead to the same metal loading. Perhaps most interesting, a protocol used to generate Cu-MOR for methane to methanol studies led to the most active catalyst both on a unit mass or unit mole copper basis. This points to a yet not recognized means to tailor catalyst activity as the open literature is silent on this issue.

Introduction

Emissions of environmentally harmful compounds from stationary and mobile sources are strictly regulated around the globe to minimize air pollution. Remarkable improvements have been achieved in hydrocarbon, CO, and NO_x abatement from gasoline-powered vehicles since the introduction of the "three-way" catalyst. However, the "three-way" catalytic converter has limited capability of reducing NO_x emissions of diesel-powered vehicle engines.[1] NO_x is a harmful gas with potential serious health repercussions. The transportation sector is a major source of NO_x emissions and significant research has been performed on the development of a new NO_x emission control technology.[2] The highly dynamic operational conditions of mobile applications require a catalyst design with high activity and hydrothermal stability. V/Ti and Fe-zeolites based catalyst systems were proposed as alternatives but were not commercially successful due to their low activity and activity dependence on feed gas composition in the low operational temperature region.[3,4] In the 1980s–2000s, Cu-ZSM-5 was discovered and explored for NO reduction due to its high activity and stable catalytic performance.[5,6] However, the issues of hydrothermal instability, reduced activity in the lower temperature region, and high hydrocarbon poisoning of Cu-ZSM-5 soon arose.[7,8] A search for more reliable zeolite hosts resulted in the discovery of small-pore zeolite chabazite (CHA).[9–11] Copper exchanged chabazite, specifically Cu-SSZ-13, has demonstrated superior catalytic activity and stability compared to other candidates and has been subsequently commercialized.[3,12,13] The success of Cu-SSZ-13 for the selective

[a] Dr. A. Koishybay, Prof. Dr. D. F. Shantz
Department of Chemical and Biomolecular Engineering
Tulane University
6823 St. Charles Avenue, New Orleans, LA 70118, USA
E-mail: dshantz@tulane.edu
[b] Mr. C. Umhey, Mr. K. Groden, Prof. Dr. J.-S. McEwen
The Gene and Linda Voiland School of Chemical Engineering and Bioengineering
Washington State University
Pullman, WA 99164, USA
[c] Dr. C.-T. Kuo, Prof. Dr. A. M. Karim
Department of Chemical Engineering
Virginia Polytechnic Institute and State University
Blacksburg, VA 24061, USA
[d] Prof. Dr. J.-S. McEwen
Department of Physics and Astronomy
Washington State University
Pullman, WA 99164, USA
[e] Prof. Dr. J.-S. McEwen
Department of Chemistry
Washington State University
Pullman, WA 99163, USA
[f] Prof. Dr. J.-S. McEwen
Department of Biological Systems Engineering
Washington State University
Pullman, 99164, USA
[g] Prof. Dr. J.-S. McEwen
Institute for Integrated Catalysis
Pacific Northwest National Laboratory
Richland, WA 99354, USA

Supporting information for this article is available on the WWW under https://doi.org/10.1002/cphc.202300271

catalytic reduction (SCR) of NO_x and the structural simplicity of the CHA topology for basic research has incited considerable interest from academic and industrial research groups. As a result, it has been revealed that metal speciation in the CHA framework is more complex than the initial assumption of a single-site catalyst.[4] As of today, a more comprehensive understanding on structural dynamics of the Cu-SSZ-13 catalyst has emerged due to the utilization of advanced in situ/*operando* characterization techniques on a well-defined set of samples under well-controlled measuring conditions.[4,13]

There is a scientific consensus that four factors strongly affect Cu-speciation in Cu-CHA: catalyst activation, composition, temperature and gas composition. The distribution of different Cu-species in Cu-SSZ-13 will vary significantly depending on the catalyst activation in the presence of oxygen versus in an inert atmosphere or under vacuum.[14–17] Martini and co-workers have demonstrated the effect of composition and temperature on the distribution of $Z_2Cu(II)$, ZCu(I) and Z[Cu(II)OH] species.[18] It has been discovered that solvating ligands such as NH_3 and H_2O can mobilize Cu-species and the Cu mobilization phenomenon has been confirmed separately by Giordanino et al. and Paolucci et al.[19,20]

Despite considerable progress in understanding the nature of active Cu species, there are several open questions that remain regarding the underlying SCR mechanism.[20–26] Such questions arise partly from the difficulty in deconvoluting the associated X-ray absorption spectra, which depends not only on the oxidation state of Cu, but also on its ligand environment.[24] As a result, a large variation in activation energy (35–139 kJ/mol) has been observed for the standard NH_3-SCR reaction.[20,23,27–35] Another common (and potentially related) observation across the SCR literature is that most of the academic and industrial research groups have their own procedure for the copper exchange of the zeolite. Perhaps surprisingly, the open literature is silent on how this might (or might not) affect the catalytic properties of the catalyst. Given the points above, it was decided to investigate how SCR behavior, especially at temperature below 200 °C, change as one uses different methods (salt identity, exchange temperature, etc.) to load copper into the zeolite.

In this work, four different solution copper-ion exchange procedures from four active groups in the field were employed to prepare Cu-SSZ-13 samples from an identical SSZ-13 parent material.[33,36–38] The resulting samples were tested for the SCR reaction under the same operational conditions. The variation in distribution of copper species across the samples was investigated using CO as a probe molecule. It has been previously shown that CO can be used to probe Cu cations coordinated in 6-membered rings (MRs) and 8MRs.[14,39,40] The catalytic activity and copper coordination environment results show unequivocally that different solution copper ion exchange procedures result in different catalyst materials, *even in the case where different protocols lead to the same metal loading.* This finding is discussed in the context of the copper speciation reported by the groups' whose protocols were used.

Experimental Section

Materials

N,N,N-trimethyl-1-adamantylammonium hydroxide (TMAdaOH, 25 wt%, SACHEM) Ludox® HS-40 colloidal silica (40 wt% suspension in water, Sigma Aldrich), aluminum hydroxide (reagent grade, Sigma Aldrich), and sodium hydroxide pellets (ACS grade, VWR) were used as received in the zeolite synthesis. Ammonium nitrate was obtained from Acros Organics (99%) and used for ammonium ion exchange. Copper (II) nitrate hemi(pentahydrate) (98%, Alfa Aesar), copper (II) sulfate pentahydrate (99%, Alfa Aesar), and copper (II) acetate (anhydrous, 98%, Alfa Aesar) were used for copper ion exchange

Zeolite synthesis. The parent SSZ-13 zeolite ($SiO_2/Al_2O_3 = 15$) was synthesized using a procedure described by Di Iorio and Gounder which is a modified version of the original synthesis reported by Zones.[41] The synthesis gel molar composition was 1 SiO_2/0.133 Al_2O_3/0.25 TMAdaOH/0.25 Na_2O/44 H_2O. As an example, 8.865 g of TMAdaOH was dissolved in 8.090 g of deionized water (18 MΩ) and stirred for 15 minutes. 0.109 g of aluminum hydroxide and 1.284 g of 5 M NaOH aqueous solution were added to the solution. The mixture was stirred for another 15 minutes before adding 3.15 g of colloidal silica. The final mixture was stirred at room temperature for 2 h, then transferred to a Teflon-lined stainless-steel autoclave and placed in an oven for 6 days at 160 °C in a rack rotating at approximately 60 rpm. The solids were recovered by vacuum filtration, washed with a copious amount of deionized water, and dried at room temperature overnight. The as-made sample was calcined in air at 550 °C for 8 h to ensure complete combustion of any occluded organic structure directing agents.

After calcination, all samples were converted to the NH_4-form by ion exchanging them with 250 mL of 0.1 M aqueous solution of NH_4NO_3 per gram of SSZ-13 at 80 °C for 8 h. The solids were recovered by vacuum filtration, washed with deionized water, and dried at room temperature overnight. The H-form of SSZ-13 was obtained by calcination of NH_4-SSZ-13 in air at 550 °C for 4 h.

Copper ion-exchange methods. Copper exchanged SSZ-13 samples were prepared using four procedures described in the literature. The protonic form of SSZ-13 was used for copper ion exchange. The first solution ion exchange procedure was adopted from Albarracin-Caballero et al. where 1 g of H-SSZ-13 was ion exchanged with 150 mL of 0.2 M $Cu(NO_3)_2$ at room temperature for 4 h.[33] The product was collected via centrifugation, reserving the supernatant, washing and re-suspending in deionized water three times to bring the pH to approximately 7. The centrifuge tube containing the wet solids was placed in the oven at 80 °C overnight until dry. The final product was labeled as Cu-SSZ-13(A–H-x) where x is the Cu/Al ratio of the product.

The second method was prepared using a recipe described by Fickel et al. where 1 g of H-SSZ-13 was ion exchanged with 500 mL of 0.1 M $CuSO_4$ at 80 °C for 1 h.[36] The product was recovered by vacuum filtration, reserving the supernatant, and washed with excess deionized water to bring the pH to approximately 7. The wet solids were placed in the oven at 80 °C overnight until dry. The final product was labeled as Cu-SSZ-13(F–H-x) where x denotes the Cu/Al ratio of the product.

The third method was adopted from a procedure described by Grundner et al.: 1 g of H-SSZ-13 was ion exchanged with 60 mL of 0.01 M $Cu(CH_3COO)_2$ at room temperature for 20 h.[38] The solids were collected via centrifugation, reserving the supernatant, washing and re-suspending in deionized water three times to bring the pH to approximately 7. The centrifuge tube containing the wet

product was placed in the oven at 80 °C overnight until dry. The final product was labeled as Cu-SSZ-13(G–H-x) where x denotes the Cu/Al ratio of the product.

The last procedure was prepared using a recipe by Kwak et al. where 1 g of H-SSZ-13 was ion exchanged with 10.2 mL of 0.1 M $Cu(NO_3)_2$ at room temperature for 24 h.[37] The solids were collected via centrifugation, reserving the supernatant, washing and re-suspending in deionized water three times to bring the pH to approximately 7. The centrifuge tube containing the wet product was placed in the oven at 80 °C overnight until dry. The final product was labeled as Cu-SSZ-13(K–H-x) where x denotes the Cu/Al ratio of the product.

Given the multiple exchange protocols used a consistent nomenclature for the samples was used where the materials are denoted as Cu-SSZ-13 (A–B-c) where A denotes the exchange method (A=Albarracin, F=Fickel, G=Grundner, and K=Kwak), B is the form of the zeolite (e.g., H^+ form), and c is the Cu/Al ratio of the resulting zeolite.

Characterization

X-ray diffraction (XRD) measurements were performed with a Rigaku MiniFlex 600 diffractometer with Cu Kα radiation over a range of 4–50° 2θ. Nitrogen adsorption experiments were performed on a Micromeritics ASAP 2020 at 77 K using approximately 50 mg of a sample. Energy-dispersive X-ray spectroscopy (EDAX) chemical analyses were obtained on a Hitachi 3400 electron microscope. Chemical analyses were performed by Galbraith Laboratories. The NO conversion measurements were performed on a Nicolet iS50R FTIR spectrometer equipped with 2.4 m heated gas cell (Pike Technologies) which was connected to the outlet of the reactor.

Diffuse-reflectance infrared Fourier-transform spectroscopy (DRIFTS) was used to characterize the interaction of the Cu-SSZ-13 samples with CO. The in situ DRIFTS experiments were performed using a Thermo Scientific IS-50R FTIR equipped with an MCT/A detector. A spectral resolution of 4 cm^{-1} was used to collect spectra, which are reported in the Kubelka–Munk (KM) units. Approximately 50 mg sample (25-90 μm diameter particles) was loaded in the Harrick Praying Mantis high-temperature DRIFTS reaction chamber. The chamber was sealed and connected to a flow system with temperature control, and gases were flown through the sample at atmospheric pressure. Each reported spectrum is an average of 32 scans. The Cu-SSZ-13 samples were pretreated in situ in 2% O_2 (99.999% Airgas) in N_2 at 550 °C for 30 min then cooled down in pure N_2 to 35 °C. Since the samples were purged and cooled, it is anticipated that the autoreduction of Cu(II) to Cu(I) will occur as it was observed in other studies[42]. We do note that there is a difference between the treatments for IR and activity measurements, namely, in the IR measurements we cool down in inert where autoreduction of Cu occurs while before activity measurements the samples are cooled in O_2. Despite this difference, this treatment procedure (in inert versus O_2 environment) will only affect the relative concentration of Cu(I) species but, as was shown in the literature,[14] will not affect the type of Cu(I) species present.

A spectrum under N_2 after the pretreatment was collected as the background for each sample. After pretreatment, 2.5% CO flowed through the sample for 10 min then purged with pure N_2 to remove gas phase CO while a series of spectra were collected continuously. Unless otherwise mentioned, the reported spectra were recorded after 4 minutes of N_2 purge. The N_2 gas was supplied from house-liquid N_2 boil-off and then further purified using high-capacity moisture and oxygen traps (Cat. #21997 and Cat. #20601, Restek). The CO (5% CO, balance N_2, certified grade Airgas) gas line was equipped with a metal carbonyl purifier (Matheson, NanoChem Metal-X) to remove trace metal carbonyls. All feed gas flows were controlled by mass flow controllers (5850EM, Brooks Instrument).

Density Functional Theory Calculations

All theoretical calculations were performed using closed-shell density functional theory implemented in the Vienna Ab initio Simulation Package (VASP).[43,44] Valence Kohn–Sham states were expanded in a plane-wave basis set using a cutoff energy of 400 eV. Their interactions with core electronic states (under the frozen-core approximation) were accounted for using the projector augmented wave method.[45,46] The PAW potentials used in this approach were released by VASP developers in 2012. To treat electronic exchange and correlation, two different functionals were employed to determine the effect of different DFT functionals on the calculational results. As such, we compare our results using the vdW-DF2[47] functional to those obtained using the PW-91 functional.[48] Fast Fourier Transform (FFT) grids used in these calculations were generated using the "Accurate" precision setting within the VASP code. To sample the first Brillouin zone, a Gamma point was considered sufficient and integration of said zone was performed using Gaussian smearing with a smearing width of 0.2 eV. Self-consistent field cycles to determine the electron density of the system were considered converged once the total energy difference between subsequent minimization steps was less than 1×10^{-8} eV. Geometries were considered converged once Hellmann-Feynman forces on all Cartesian degrees of freedom were less than 0.02 eV/Å. Vibrational frequencies were generated with second-order finite differences (step size 0.01 Å) to compute the elements of the Hessian matrix using in-house software wrapped around VASP.

The unit cell volume was determined in our previous work using a three-step procedure.[49,50] This gives an equilibrium volume of 845.1 $Å^3$ ($a = 9.2$ Å $b = 9.5$ Å $c = 9.6$ Å $\alpha = 92.8°$, $\beta = 92.1°$, $\gamma = 93.7°$) using the vdW-DF2 functional. We present an energy-volume curve in the Supporting Information that shows the results of this procedure for our loaded SSZ-13 unit cell. Using the PW-91 functionals, we obtain an optimized volume of 823.6 $Å^3$. Details of the optimized unit cell using the PW-91 functional can be found in our previous work.[50] Both optimized volumes are approximately rhombohedral, when a Si atom is replaced with one Al atom and charge compensated by a Cu(I) cation. This unit cell is denoted as ZCu, which is larger than the SSZ-13 zeolite and consistent with the results reported by McEwen et al.[49] Five models where constructed in our work: two models where a CO molecule is adsorbed on a Cu(I) cation at the two possible 8-membered ring site locations (denoted as the 8MR_O14 and the 8MR_O24 sites in our previous work[50]), another where CO is adsorbed on a Cu(I) cation that is located in a 6-membered ring where one Al is located in the 6-membered ring. Several other models were constructed where two Al species are located within a 6-membered ring (with one or two Si separating the two Al), which are charge compensated with a Brønsted acid site and a Cu(I) cation.

Catalytic Testing

The SCR activity of samples was tested in a packed bed flow reactor system using gas mixtures containing 350 ppm NO, 350 ppm NH_3, 14% O_2, and 2% H_2O with a balance of N_2. 100 mg of catalyst powder with a nominal size of 180–250 μm was loaded in a $^1/_4$" OD quartz tube, which was then placed inside an electric furnace. Prior to the catalytic testing, the samples were pretreated at 550 °C under flowing air for 30 min to remove trace gases. The total flow rate was held at 50 sccm to achieve the gas hourly space velocity

(GHSV) of ~30,000 h^{-1}. The higher GHSV (~135,000 h^{-1}) was achieved by using 30 mg catalyst and 71.4 sccm total flow rate. The NO_x conversions as a function of temperature are defined as $((NO_{inlet}-NO_{outlet})/NO_{inlet})x100$. The fixed copper loading SCR activity of Cu-SSZ-13 samples was tested using catalysts containing 0.235 mg of copper in the reactor. The catalyst bed was diluted with 46 grit SiC chips to achieve a GHSV of ~30,000 h^{-1}. SiC was tested prior for SCR activity and was catalytically inactive. The SCR reaction was deemed to reach steady state at each temperature before collecting several IR spectra. The NO conversion results were calculated by integrating and averaging the NO peak area and comparing to calibration curves generated in house. The conversions shown are determined by the integration of multiple (at least five) spectra once steady state is obtained. Error bars are shown on all points.

Results and Discussion

Catalyst Properties

To directly compare the effects of the ion exchange, a parent SSZ-13 material was used throughout. The Supporting Information contains the powder X-ray diffraction (PXRD) pattern, nitrogen porosimetry isotherm, and a representative SEM image. Unit-cell refinement of the PXRD pattern shows the material is phase pure (13.682×13.682×14.803 $Å^3$). Nitrogen porosimetry shows a typical Type I isotherm and a micropore volume of 0.27 cm^3/g based on analysis using the t-plot method (Figure S1). FE-SEM shows the materials are cubes with a typical size of 0.5 μm per edge (Figure S2). ICP-OES analysis performed by Galbraith gives a SiO_2/Al_2O_3 ratio of 15.4±0.1. By comparison, SEM-EDS gives a SiO_2/Al_2O_3 ratio of 14.7±0.1. The conclusion is that from sample to sample and batch to batch we are starting with highly similar parent SSZ-13 materials.

Table 1 shows the conditions used and Cu/Al of the obtained materials as determined by EDS and confirmed by ICP analysis by Galbraith Laboratories. The immediate conclusions are that the different protocols lead to a large variation of the Cu/Al ratio. It is also worth noting the large range of conditions used in the SCR research space to load copper into SSZ-13.

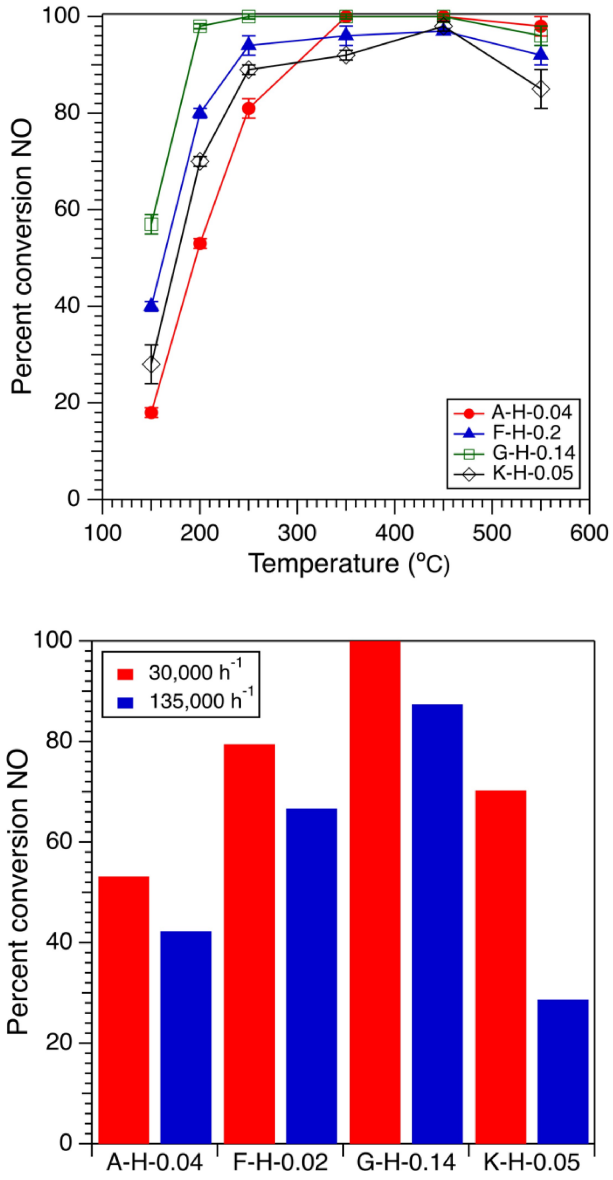

Figure 1. (Top) NO conversion profiles for Cu-SSZ-13 samples at a fixed mass of catalyst at a space velocity of 30,000 h^{-1}. (Bottom) Effect of space velocity on NO conversion at 200 °C.

SCR Activity at Fixed Catalyst Loading in the Reactor

Figure 1 shows the light off curves for the four Cu-SSZ-13 samples. It should be noted that under the same conditions SiC chips show no SCR activity, and SSZ-13 without copper is inactive below 400 °C. Cu-SSZ-13(A–H-0.04) has the lowest conversion at low (< 250 °C) temperatures as compared with the other samples. It has the lowest Cu/Al ratio which is one explanation for the observed low catalytic activity. However,

Table 1. Ion exchange conditions used. Per the experimental section, the nomenclature of the samples is Cu-SSZ-13 (A–B-c), where A identifies the protocol used, B is the form of the zeolite used, and c is the Cu/Al ratio of the resulting product.

Sample label	Copper salt used	Volume [mL] (concentration)/g-zeolite	pH initial	pH final	Mixing conditions	Cu/Al	Ref.
Cu-SSZ-13(A–H-0.04)	$Cu(NO_3)_2$	150 (0.2 M)	3.73	3.03	4 h, RT	0.04	[33]
[Cu-SSZ-13(F–H-0.2)	$CuSO_4$	500 (0.1 M)	3.50	3.00	1 h, 80 °C	0.20	[36]
[Cu-SSZ-13(G–H-0.14)	$Cu(CH_3COO)_2$	60 (0.01 M)	5.88	4.74	20 h, RT	0.14	[38]
[Cu-SSZ-13(K–H-0.05)	$Cu(NO_3)_2$	10.2 (0.1 M)	3.94	2.11	24 h, RT	0.05	[37]

Cu-SSZ-13(H–G-0.14) has the highest activity though Cu-SSZ-13(F–H-0.2) has higher copper content. As can be seen in Figure 1, all samples show similar catalytic activity in the 350–550 °C temperature window. At temperatures below 350 °C, the reaction takes a different catalytic path in each sample (Figure 1).[1,28,30] Although the pathway was proposed to be different in the low temperature regime (where NH_3 solvates and liberates Cu ions from direct association with the zeolite support, and these solvated Cu ions act as the redox-active catalytic sites[19,20]), these results suggest that the different ion exchange protocols lead to different copper speciation, as samples with similar copper content show different reactivity, and the most active sample is in fact not the one with the most copper. Such a difference in Cu speciation in solution during deposition will also influence the starting Cu(I)/Cu(II) ratio.

Also included in Figure 1 is the NO conversion at 200 °C for the samples tested at space velocities of 30,000 h^{-1} and 135,000 h^{-1}. As anticipated the conversion is lower for all samples at the higher space velocity, with the Kwak sample K–H-0.05 showing the largest change. The high GHSV (135,000 h^{-1}) results are consistent with the low GHSV (30,000 h^{-1}) results. The catalytic activity decreases in the following order for the four samples at high GHSV: Cu-SSZ-13(G–H-0.14) > Cu-SSZ-13(H–F-0.2) > Cu-SSZ-13(A–H-0.04) > Cu-SSZ-13(K–H-0.05). The Cu-SSZ-13(A–H-0.04) and (K–H-0.05) samples have similar Cu/Al ratios. However, these two samples have different catalytic activities at different conditions. Cu-SSZ-13(K–H-0.05) shows better conversion at lower GHSV as compared with Cu-SSZ-13(A–H-0.04). This again could be pointing to different copper speciation in the samples. This will be addressed in more detail below using IR and H_2 TPR. All Cu-SSZ-13 samples showed formation of N_2O at levels below 5 ppm over the temperature range studied (Figure S3 and S4).

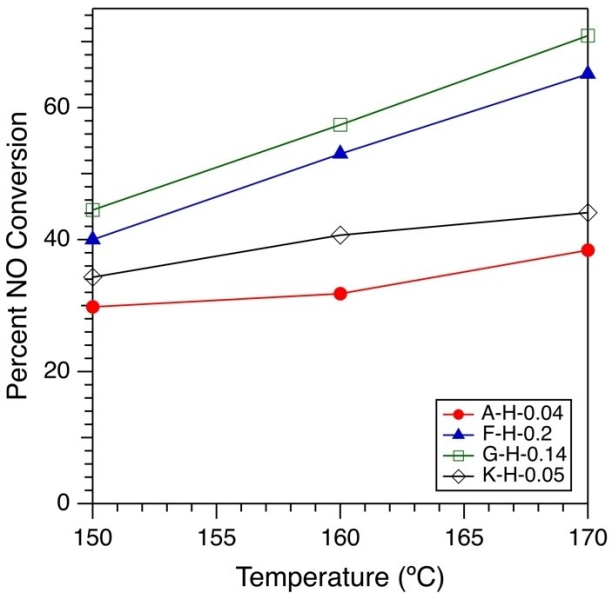

Figure 2. NO conversion over the temperature range of 150–170 °C for all the measured samples at a fixed copper content (0.235 mg) in the reactor.

SCR Activity at fixed Cu Loading in the Reactor

The results above, per prior literature, are in general consistent with the idea that increased copper content leads to a higher SCR activity. But while the results indicate that different exchange protocols lead to different copper loadings, it could also be that the different protocols lead to different copper speciation which at least in part explains the differences observed in Figure 1. To determine if the different samples are *intrinsically* more active on a unit copper basis, experiments were performed where the amount of zeolite was varied in the reactor (diluted with silicon carbide chips) so that each run had a fixed amount of copper (0.235 mg). Figure 2 shows clear differences between the two low content copper samples and the two higher (Cu/Al > 0.1) copper content samples. However, note for the results in Figure 2 that the mass of copper in the reactor was constant across the four different samples. This suggests that the different ion exchange processes lead to samples with copper with intrinsically different sites in terms of SCR activity. One potential cause for this could be the ion exchange processes lead to different copper speciation/siting, including different oxidation states and clusters (e.g., copper oxo clusters). This is explored in more detail below (see below). In this context, it is also worth noting that all exchanges except the Grundner are at solution pH values below 4, whereas the Grundner exchange method is at a pH just below 6. Another possible explanation is the existence of regions with a higher density of copper sites in the zeolites with higher initial copper loadings. Prior research has suggested increasing the density of copper sites increases the kinetic relevance of the reduction of Cu(II) and decreases the kinetic relevance of Cu(I) oxidation leading to an increase in SCR activity at ambient pressures and 473 K.[51]

SCR activity of low Cu/Al samples. As can be seen above, the Kwak (K–H-0.05) and Albarracin (A–H-0.04) preparation protocols lead to Cu/Al values below 0.1 and are both less active on a mass zeolite basis as well as a mass copper basis than the other two samples. To attempt to explore this further, the Grundner protocol was modified to produce a zeolite with a Cu/Al = 0.03 and tested at the same conditions as those used for the samples shown in Figure 1 (i.e., fixed mass of catalyst). The light-off curves for these three samples are shown in Figure 3. There is a pronounced drop in the activity of the G–H-0.03 sample as compared to the G–H-0.14 sample, and this sample appears less active than the other two. Moreover, considering the G–H-0.03 sample results in Figure 3, this sample has a comparable amount of copper in the reactor as the results for G–H-0.14 in Figure 2. As can be seen from Figure 2, the G–H-0.14 sample has a conversion of 44% at 150 °C whereas the G–H-0.03 sample has negligible conversion at 150 °C and only approximately 32% conversion at 200 °C. This result, consistent with the conclusions above, suggests that the two G–H-x samples have different copper species in them. It is interesting to note however, that in the work by Grundner[38] they invoke the formation of copper trimers to be effectively

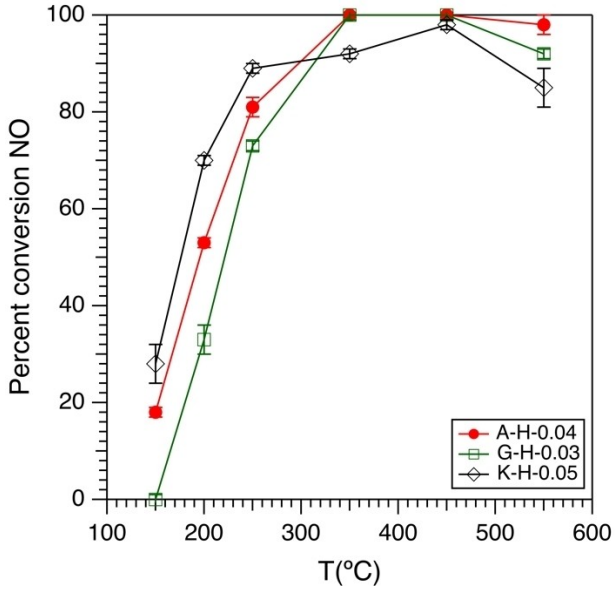

Figure 3. NO conversion versus temperature for samples with low (Cu/Al <0.1) copper content at a constant mass of catalyst at a space velocity of 30,000 h^{-1}.

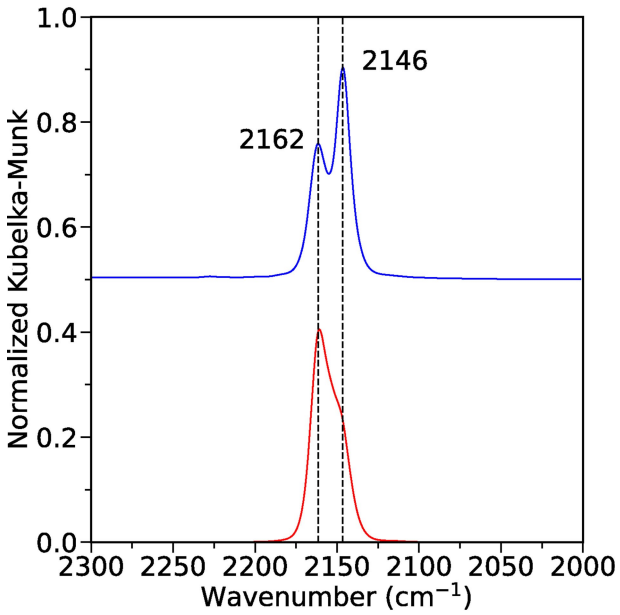

Figure 4. IR of CO adsorbed on (top) A–H-0.04 and (bottom) G–H-0.14.

independent of copper loading. That does not appear to be the case here, perhaps a result of the different zeolite pore topologies, as the Grundner work explored mordenite zeolites.

Probe Molecule Binding Studies

DRIFTS of CO adsorption on Cu was used to characterize the interaction of CO with Cu and determine if the ion-exchange protocol affects the type of Cu species in the samples. Figure 4 shows the DRIFTS spectra of CO adsorbed on the most active and the least active samples when tested at a constant copper content in the reactor (G–H-0.14 and A–H-0.04 as shown in Figure 3). The spectra for the other samples are in the Supporting Information (Figure S7–S9). Two CO bands (shoulder for A–H-0.04 and G–H-0.14) associated with adsorption of CO on Cu(I) can be clearly seen on all the samples at ~2145-2147 and 2159–2162 cm^{-1} (see, for example, Figure 4 with maxima at 2062 cm^{-1} and 2046 cm^{-1}). We note that Cu(I) dicarbonyl complexes and CO adsorbed on Cu(II) were observed during CO flow on the samples (see Supporting Information). The CO band at lower wavenumber has been assigned to adsorption on Cu(I) in a more constrained environment within the zeolite as compared with the higher wavenumber band.[39,52] The different relative intensities of these two CO bands indicate differences between the samples in the Cu(I) adsorption sites within the SSZ-13 zeolite cages. Prior literature has suggested at copper loadings similar to the loadings present in our study the oxidation of Cu(I) is the dominant kinetic step.[51] This would suggest that differences in the siting of Cu(I) may explain some of the observed differences in SCR activity. To determine if the activity is correlated with the 2159–2161 cm^{-1} CO band, we deconvoluted the IR bands and calculated the areas of 2159–2161 cm^{-1} peak relative to the area of the 2145–2147 cm^{-1} peak. Interestingly, the normalized SCR activity of the samples at a fixed copper content is proportional to the relative area of the higher wavenumber CO band (2159-2162 cm^{-1}, Figure 5). The results indicate a strong effect of the location of Cu(I) site within the zeolite on the properties of copper and its activity for SCR. This dependency is clearly a function of the solution ion exchange conditions used.

To probe this issue further, H_2 temperature programmed reduction (TPR) was performed on selected samples, namely

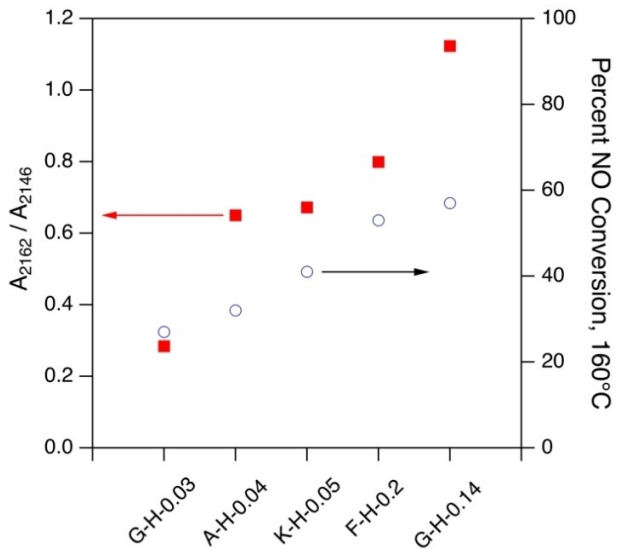

Figure 5. Ratio of the IR peak area (left axis) and percent NO conversion at 160 °C (right axis) for the samples.

the A–H-0.04 and G–H-0.14 sample, i.e., the least and most active samples respectively. Figure 6 shows the results for the two samples. In both samples there are two features, one located at approximately 210 °C and another at approximately 380 °C.

Literature assigns these respectively to copper in less stable/easier to reduce sites such as 8- membered rings (low T) and copper in more stable sites such as double six-membered rings (high T). A–H-0.04 consumes 55.9 μmol H_2/cat, 17.4 μmol is in the low T feature and 38.5 μmol is in the higher temperature feature. G–H-0.14 in contrast consumes 112.7μmol H_2/cat, and 68.4 μmol is in the low T feature and 44.3 μmol is associated with the high temperature feature. The ratios for the two samples are 0.45 and 1.54 respectively. This trend is consistent with the IR results.

DFT-based Modeling of IR Spectra and Correlation to the Experimental Results

We determined the vibrational frequencies from first principles for CO adsorbed on ZCu sites where Cu is located in one of the three 6-membered ring (6MR) site models or in one of the 8-membered ring site models (the 8MR_O14 site and the 8MR_O24 site) for comparison with the experimental IR spectra. The models and the corresponding CO stretch frequencies are shown in Figure 7. In addition to the conformations that are shown in Figure 7 in the presence of a Brønsted acid site, several other possible conformations are shown in Figure S12. As previously discussed, a CO stretching frequency shift between 12 and 17 cm^{-1} was observed in all the experimental samples. From the van der Waals data, there are three structure pairs with frequency gaps in this range, the first being a six-membered ring and an O24 eight-membered ring configuration. The second being between the two six-membered ring configurations each with the two aluminum sites being charge compensated by a Brønsted acid site and a Cu(I) cation. The third possible scenario being an O14 eight-membered ring and a six-membered ring with a two aluminum sites one of which is charge compensated by a Brønsted acid (the ZCuCO–Si-Si-ZH conformation as shown in Figure 7). Of the three potential pairs, the pair involving two six-membered rings appears the least likely. Our DFT-based model shows that the ZCuCO–Si-Si-ZH structure is more energetically favorable than the ZCuCO–Si-ZH structure both before and after CO adsorption by 0.89 eV and 0.47 eV respectively making it unlikely to observe both structures since the ZCuCO–Si-Si-ZH structure should be the dominant structure when a Brønsted acid site is included in the zeolite. Similarly, when examining the configuration with no Brønsted acid sites, the O14 configuration is slightly more favorable than the 6MR and the O24 configurations by 0.05 and 0.10 eV respectively. As such, the scenario containing the ZCuCO–Si-Si-ZH configuration and the O14 configuration contains the most favorable configurations with and without Brønsted acid sites. Additionally, when examining the copper uptake of the zeolites prepared using the Fickel method and the Kwak method, the Cu : Al ratio is 4 times higher in the Fickel sample than in the Kwak sample (Table 1). A plausible explanation of these results is the Kwak sample has a larger number of conformations in which Al is charge compensated with species other than copper as compared to the Fickel sample. This would result in the Kwak sample having a lower CO stretch frequency than in the Fickel sample. This scenario can only be explained by the high frequency O14 and low frequency ZCuCO–Si-Si-ZH pair since the other potential pairs do not vary their Al to Cu ratio. As such, we associate the higher wavenumber IR frequency as found in the F–H-0.2 sample to Cu being located in an 8-membered ring with the Cu being located in an 8MR_O14 site. Additionally, we associate the lower wavenumber IR peak in the K–H-0.05 sample with Cu(I) being in a six-membered ring in the presence of 2 Al species where one of the Al species is charge compensated by a Brønsted acid site with two silicon atoms separating the Al sites. The comparison between these DFT-based frequencies and the experimental values are shown in Figure 8, where the DFT-based frequency values where uniformly shifted for ease of comparison. Based on adsorption energies the O_14 site is more favorable than the ZCuCO–Si-Si-ZH site by 0.7 eV (Table S2) suggesting the CO will preferentially adsorb in O_14 locations until they become unavailable and then begin to adsorb to ZCuCO–Si-Si-ZH sites. These results also support our TPR data from the G–H-0.14 sample and the A–H-0.04 sample. The TPR data indicates the G–H-0.14 sample has a prevalence of copper in 8MR sites while the A–H-0.04 has more copper in harder to reduce sites such as D6MR. Looking at the IR spectra for both samples we see the G–H-0.14 sample has a peak at 2162 cm^{-1} which we associate with copper in an 8MR site and the A–H-0.04 sample has a peak at 2146 cm^{-1} which we associate with copper in a 6MR site, as illustrated in inserts in Figure 8.

Interestingly, the C–O bond length is only 0.002 Å longer in the Brønsted acid conformation in a 6MR as compared to when CO is adsorbed in an 8MR_O14 site. In Figure 8, we visually compare the CO frequency for the 2 Si species-separated model and the 8MR_O14 model to the experimental results. Changing the functional from the vdW-DF2 to PW-91 functional slightly

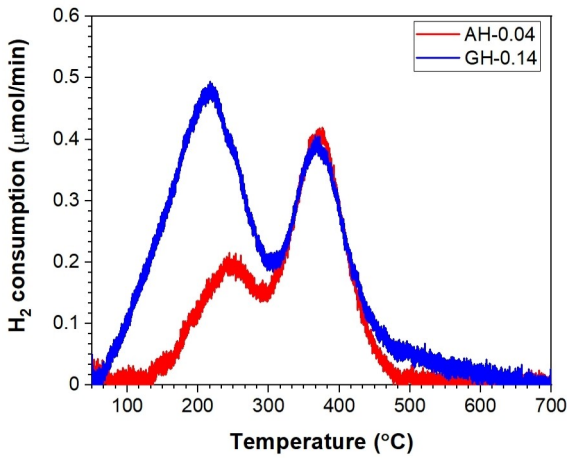

Figure 6. Hydrogen temperature programmed reduction curves for A–H-0.04 (red) and G–H-0.14 (blue).

Name	Structure (Top View)	Structure (Side View)	vdW-DF2 CO Stretch Freq cm^{-1}	vdW-DF2 CO bond distance (Å)	PW-91 CO Stretch Freq cm^{-1}	PW-91 CO bond distance (Å)
Z-CuCO (6MR)	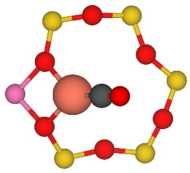	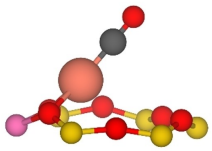	2079.5	1.147	2115.5	1.148
Z-CuCO (8MR-O14)	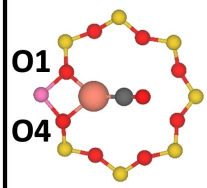		2086.1	1.146	2116.8	1.148
Z-CuCO (8MR-O24)	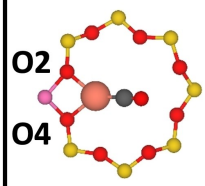	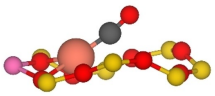	2093.6	1.145	2122.5	1.147
ZCuCO-Si-ZH (6MR)	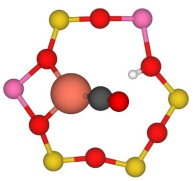	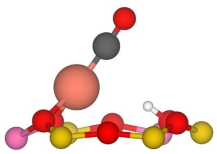	2084.2	1.146	2115.5	1.148
ZCuCO-Si-Si-ZH (6MR)	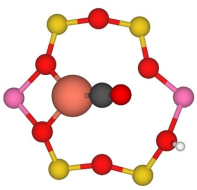	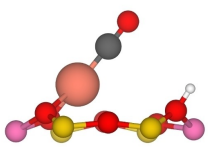	2071.1	1.148	2109.0	1.149

Figure 7. Structures, CO stretch frequencies, and CO bond distances for a selection of geometries where CO adsorbed on a Cu(I) cation in the SSZ-13 lattice. The red, yellow, pink, brown and grey spheres are oxygen, silicon, aluminium, copper and carbon atoms, respectively.

changed the results, however the overall findings are very similar. Using the PW-91 functional the low IR frequency was attributable to the exact same structure described previously and the high wavenumber IR peak was still attributed to the Cu(I) being located in an 8 membered ring, however with the PW-91 functional the Cu(I) was located in an O_24 site instead of an O_14 site identified using the vdW-DF2 functional.

These results indicate that the site where Cu sits in the zeolite (e.g., 6 or 8 membered ring), the distribution of the Brønsted acid sites in the two samples and the Cu distribution among the different sites are strongly dependent on the ion exchange method and the initial form of the parent zeolite.

Physical Picture

The work described above clearly shows that *how* copper is loaded into SSZ-13 has a clear impact on the SCR behavior of the catalyst, even when samples made using different protocols have similar copper loadings. This has not been widely discussed or appreciated in the open literature. This, we believe, is the most important finding of the work as it gives the community another design parameter for tuning reactivity. Thus, an important question is do these different protocols lead to different metal speciation? While an exhaustive study of all the systems with X-ray absorption spectroscopy (XAS) is beyond

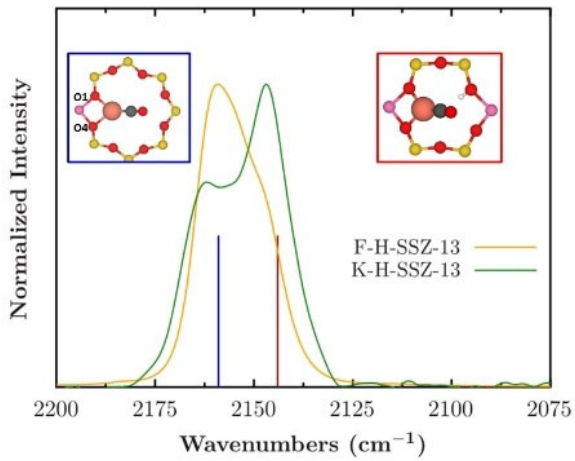

Figure 8. Experimental IR spectra showing sensitivity of the Cu cation location on the synthesis procedure used for the K–H-0.05 sample (Kwak H-SSZ-13) and the F–H-0.2 sample (Fickel H-SSZ-13). The blue line is for CO adsorbed on Cu(I) in an 8-membered ring and the red line is for CO adsorbed on Cu(I) in a 6-MR ring with a Brønsted acid site directly across the hexagonal ring. The theoretical CO stretch frequencies were uniformly shifted so that the 8MR frequency aligned with the maxima of the experimental Fickel spectra. The sphere legend is the same as Figure 7.

the scope of this study, we can draw some conclusions based on the literature from which the protocols were taken. First, the exchange protocol from the Grundner paper was used to exchange copper into mordenite zeolites and the authors made a strong case that copper trimers were in fact the active species.[38] Subsequent work by the same group has at least partially walked back the claim of copper trimers in MOR[54]. By contrast, the work by Fickel and Lobo invoked isolated copper species.[36] It should be noted that the work by Fickel and Lobo investigated copper in dehydrated SSZ-13 materials that were higher in aluminum content (Si/Al = 6) than those studied here. The same is true of the work by Kwak and coworkers. Subsequent work by that lab.[53] reports that under reaction conditions the Cu(II) species (unless under dehydrated conditions) are in the cages of the zeolite and not strongly associated with the framework. However, consistent with this work they claim that the Cu(I) species are associated with the eight membered rings. Their work is silent on the nuclearity of the clusters. The work reported by Albarracin and coworkers invokes isolated Cu(II) species on their Cu-SSZ-13 samples based on NH_3 titration and UV-Vis experiments.[33] Given the clearly higher activity of the Grundner samples at low temperatures on a fixed copper basis (Figure 2), the simple conclusion is that this higher pH exchange which is reported to lead to copper trimers generates the most active catalyst. We cannot state that in the current work we in fact have copper trimers, and in fact the recent paper of Lercher and coworkers[54] calls the trimers picture into question, as in-depth analysis of the XAS measurements leads to the invocation of dimers. Finally, while none of these papers invoke larger clusters, we cannot definitively rule them out. What is clear in the current work however, is the Cu-SSZ-13 generated from that prep leads to the most active catalyst on both a 'mass catalyst' (Figure 1) and 'mass copper' (Figure 2) basis. Indeed, the presence of isolated Cu species are invoked in the work of Fickel,[36] while the reported nuclearity changes in the work of Grundner[38] and the more recent work of Lercher and coworkers,[54] which follows a different synthesis protocol than that of Fickel. Further ongoing work is exploring this further and will be explore elsewhere.

Conclusions

Four Cu-SSZ-13 samples were prepared using four copper exchange protocols reported in the literature and tested for SCR of NO. SCR activity results clearly demonstrated that the different exchanges led to both different copper uptake but also different copper speciation. DRIFTS IR of CO adsorbed in the various Cu-SSZ-13 samples confirm this, based on the relative peak areas of two different features, one at 2146 and the other at 2162 cm^{-1}. DFT calculations performed show that the different spectroscopic fingerprints are due to CO bound to Cu(I) in an eight (2162 cm^{-1}) or six (2146 cm^{-1}) membered ring. The results provide clear evidence that the details of the ion-exchange protocol impacts SCR behavior, a finding not previously appreciated by the SCR community. These results point to using ion exchange conditions as a means to moderate the population of different copper species in zeolites for SCR and other applications.

Author Contributions

Aibolat Koishybay: NO conversion and temperature programed reduction measurements, Writing-Original draft preparation Chun-Te Kuo: IR Measurements Charles Umhey: Computations, Writing-Reviewing and Editing Kyle Groden: Computations Jean-Sabin McEwen: Supervision, Writing-Reviewing Editing Ayman Karim: Supervision, Writing-Reviewing Editing Daniel F. Shantz: Conceptualization, Writing-Reviewing Editing

Acknowledgements

AMK and C-TK acknowledge funding from the American Chemical Society Petroleum Research Fund under award number PRF# 55575-ND5. DFS acknowledges funding from the American Chemical Society Petroleum Research Fund Award #57697-ND5 which partially supported this work. The DFT-based calculations in the paper were performed in the Environmental Molecular Sciences Laboratory (EMSL), a national scientific user facility sponsored by the DOE's Office of Biological and Environmental Research and located at PNNL. Financial support to WSU was partly provided by the National Science Foundation CAREER program under contract No. CBET-1653561. Financial support to WSU was also partly provided by the National Science Foundation under contract No. CBET-2035280. PNNL is operated for the US DOE by Battelle.

Conflict of Interests

The authors declare no conflict of interest.

Data Availability Statement

The data that support the findings of this study are available from the corresponding author upon reasonable request.

[1] A. M. Beale, F. Gao, I. Lezcano-Gonzalez, C. H. F. Peden, J. Szanyi, *Chem. Soc. Rev.* **2015**, *44*, 7371–7405.
[2] V. Franco, F. P. Sánchez, J. German, P. Mock in Real-world exhaust emissions from modern diesel cars, Vol. (Ed. Eds.: Editor), The International Council on Clean Transportation, City, **2014**.
[3] M. Dusselier, M. E. Davis, *Chem. Rev.* **2018**, *118*, 5265–5329.
[4] E. Borfecchia, P. Beato, S. Svelle, U. Olsbye, C. Lamberti, S. Bordiga, *Chem. Soc. Rev.* **2018**, *47*, 8097–8133.
[5] M. Iwamoto, H. Furukawa, Y. Mine, F. Uemura, S. I. Mikuriya, S. Kagawa, *J. Chem. Soc. Chem. Commun.* **1986**, 1272–1273.
[6] C. T. Goralski, W. F. Schneider, *Appl. Catal. B.* **2002**, *37*, 263–277.
[7] K. C. C. Kharas, H. J. Robota, D. J. Liu, *Appl. Catal. B.* **1993**, *2*, 225–237.
[8] J. Y. Yan, G. D. Lei, W. M. H. Sachtler, H. H. Kung, *J. Catal.* **1996**, *161*, 43–54.
[9] S. I. Zones in Zeolite SSZ-13 and its method of preparation Vol. US4544538 A (Ed. Eds.: Editor), City, **1985**.
[10] S. I. Zones, L.-T. Yuen, J. S. Miller in Small crystallite zeolite CHA, Vol. US 6,709,644 B2 (Ed. Eds.: Editor), City, **2004**.
[11] J. H. Wang, H. W. Zhao, G. Haller, Y. D. Li, *Appl. Catal. B* **2017**, *202*, 346–354.
[12] Y. J. Kim, J. K. Lee, K. M. Min, S. B. Hong, I. S. Nam, B. K. Cho, *J. Catal.* **2014**, *311*, 447–457.
[13] F. Gao, C. H. F. Peden, *Catalysts* **2018**, *8*, 140.
[14] F. Giordanino, P. N. R. Vennestrom, L. F. Lundegaard, F. N. Stappen, S. Mossin, P. Beato, S. Bordiga, C. Lamberti, *Dalton Trans.* **2013**, *42*, 12741–12761.
[15] E. Borfecchia, K. A. Lomachenko, F. Giordanino, H. Falsig, P. Beato, A. V. Soldatov, S. Bordiga, C. Lamberti, *Chem. Sci.* **2015**, *6*, 548–563.
[16] D. K. Pappas, E. Borfecchia, M. Dyballa, I. A. Pankin, K. A. Lomachenko, A. Martini, M. Signorile, S. Teketel, B. Arstad, G. Berlier, C. Lamberti, S. Bordiga, U. Olsbye, K. P. Lillerud, S. Svelle, P. Beato, *J. Am. Chem. Soc.* **2017**, *139*, 14961–14975.
[17] B. Ipek, M. J. Wulfers, H. Kim, F. Goltl, I. Hermans, J. P. Smith, K. S. Booksh, C. M. Brown, R. F. Lobo, *ACS Catal.* **2017**, *7*, 4291–4303.
[18] A. Martini, E. Borfecchia, K. A. Lomachenko, I. A. Pankin, C. Negri, G. Berlier, P. Beato, H. Falsig, S. Bordiga, C. Lamberti, *Chem. Sci.* **2017**, *8*, 6836–6851.
[19] F. Giordanino, E. Borfecchia, K. A. Lomachenko, A. Lazzarini, G. Agostini, E. Gallo, A. V. Soldatov, P. Beato, S. Bordiga, C. Lamberti, *J. Phys. Chem. Lett.* **2014**, *5*, 1552–1559.
[20] C. Paolucci, I. Khurana, A. A. Parekh, S. C. Li, A. J. Shih, H. Li, J. R. Di Iorio, J. D. Albarracin-Caballero, A. Yezerets, J. T. Miller, W. N. Delgass, F. H. Ribeiro, W. F. Schneider, R. Gounder, *Science* **2017**, *357*, 898–903.
[21] M. Iwasaki in *Mechanistic Aspect of NO–NH_3–O_2 Reacting System, Vol.* (Eds.: I. Nova, E. Tronconi), Springer, New York, **2014**, pp.221–246.
[22] T. V. W. Janssens, H. Falsig, L. F. Lundegaard, P. N. R. Vennestrom, S. B. Rasmussen, P. G. Moses, F. Giordanino, E. Borfecchia, K. A. Lomachenko, C. Lamberti, S. Bordiga, A. Godiksen, S. Mossin, P. Beato, *ACS Catal.* **2015**, *5*, 2832–2845.
[23] F. Gao, D. H. Mei, Y. L. Wang, J. Szanyi, C. H. F. Peden, *J. Am. Chem. Soc.* **2017**, *139*, 4935–4942.
[24] R. Zhang, J.-S. McEwen, *J. Phys. Chem. Lett.* **2018**, *9*, 3035–3042.
[25] R. Zhang, H. Li, J.-S. McEwen, *J. Phys. Chem. C* **2017**, *121*, 25759–25767.
[26] N. Usberti, F. Gramigni, N. D. Nasello, U. Iacobone, T. Selleri, W. S. Hu, S. J. Liu, X. Gao, I. Nova, E. Tronconi, *Appl. Catal. B* **2020**, *279*.
[27] J. H. Kwak, D. Tran, J. Szanyi, C. H. F. Peden, J. H. Lee, *Catal. Lett.* **2012**, *142*, 295–301.
[28] F. Gao, E. D. Walter, E. M. Karp, J. Y. Luo, R. G. Tonkyn, J. H. Kwak, J. Szanyi, C. H. F. Peden, *J. Catal.* **2013**, *300*, 20–29.
[29] S. A. Bates, A. A. Verma, C. Paolucci, A. A. Parekh, T. Anggara, A. Yezerets, W. F. Schneider, J. T. Miller, W. N. Delgass, F. H. Ribeiro, *J. Catal.* **2014**, *312*, 87–97.
[30] F. Gao, E. D. Walter, M. Kollar, Y. L. Wang, J. Szanyi, C. H. F. Peden, *J. Catal.* **2014**, *319*, 1–14.
[31] F. Gao, N. M. Washton, Y. L. Wang, M. Kollar, J. Szanyi, C. H. F. Peden, *J. Catal.* **2015**, *331*, 25–38.
[32] C. Paolucci, A. A. Parekh, I. Khurana, J. R. Di Iorio, H. Li, J. D. A. Caballero, A. J. Shih, T. Anggara, W. N. Delgass, J. T. Miller, F. H. Ribeiro, R. Gounder, W. F. Schneider, *J. Am. Chem. Soc.* **2016**, *138*, 6028–6048.
[33] J. D. Albarracin-Caballero, I. Khurana, J. R. Di Iorio, A. J. Shih, J. E. Schmidt, M. Dusselier, M. E. Davis, A. Yezerets, J. T. Miller, F. H. Ribeiro, R. Gounder, *Reac. Chem. Eng.* **2017**, *2*, 168–179.
[34] Y. R. Cui, Y. L. Wang, D. H. Mei, E. D. Walter, N. M. Washton, J. D. Holladay, Y. Wang, J. Szanyi, C. H. F. Peden, F. Gao, *J. Catal.* **2019**, *378*, 363–375.
[35] W. Eijima, G. Shibata, N. Shibayama, Y. Kobashi, H. Ogawa, K. Shimizu, *Catal. Today* **2020**, *352*, 237–242.
[36] D. W. Fickel, J. M. Fedeyko, R. F. Lobo, *J. Phys. Chem. C* **2010**, *114*, 1633–1640.
[37] J. H. Kwak, R. G. Tonkyn, D. H. Kim, J. Szanyi, C. H. F. Peden, *J. Catal.* **2010**, *275*, 187–190.
[38] S. Grundner, M. A. C. Markovits, G. Li, M. Tromp, E. A. Pidko, E. J. M. Hensen, A. Jentys, M. Sanchez-Sanchez, J. A. Lercher, *Nat. Commun.* **2015**, *6*.
[39] J. H. Kwak, H. Y. Zhu, J. H. Lee, C. H. F. Peden, J. Szanyi, *Chem. Commun.* **2012**, *48*, 4758–4760.
[40] G. T. Palomino, S. Bordiga, A. Zecchina, G. L. Marra, C. Lamberti, *J. Phys. Chem. B* **2000**, *104*, 8641–8651.
[41] J. R. Di Iorio, R. Gounder, *Chem. Mater.* **2016**, *28*, 2236–2247.
[42] G. Brezicki, J. D. Kammert, T. B. Gunnoe, C. Paolucci, R. J. Davis, *ACS Catal.* **2019**, *9*, 5308–5319.
[43] G. Kresse, J. Hafner, *Phys. Rev. B Condens. Matter* **1993**, *47*, 558–561.
[44] G. Kresse, J. Furthmüller, *Phys. Rev. B Condens. Matter* **1996**, *54*, 11169–11186.
[45] P. E. Blöchl, *Phys. Rev. B* **1994**, *50*, 17953–17979.
[46] G. Kresse, D. Joubert, *Phys. Rev. B Condens. Matter* **1999**, *59*, 1758–1775.
[47] K. Lee, É. D. Murray, L. Kong, B. I. Lundqvist, D. C. Langreth, *Phys. Rev. B Condens. Matter* **2010**, *82*, 081101.
[48] J. P. Perdew, Y. Wang, *Phys. Rev. B Condens. Matter* **1992**, *45*, 13244.
[49] J.-S. McEwen, T. Anggara, W. F. Schneider, V. F. Kispersky, J. T. Miller, W. N. Delgass, F. H. Ribeiro, *Catal. Today* **2012**, *184*, 129–144.
[50] R. Zhang, J. Szanyi, F. Gao, J.-S. McEwen, *Catal. Sci. Technol.* **2016**, *6*, 5812–5829.
[51] I. K. Casey B. Jones, Siddarth H. Krishna, Arthur J. Shih, W. Nicholas Delgass, Jeffrey T. Miller, Fabio H. Ribeiro, William F. Schneider, Rajamani Gounder, *J. Catal.* **2020**, *389*, 140–149.
[52] J. Szanyi, J. H. Kwak, H. Zhu, C. H. F. Peden, *Phys. Chem. Chem. Phys.* **2013**, *15*, 2368–2380.
[53] J. H. Kwak, T. Varga, C. H. F. Peden, F. Gao, J. C. Hanson, J. Szanyi, *J. Catal.* **2014**, *314*, 83–93.
[54] I. Lee, M.-S. Lee, L. Tao, T. Ikuno, R. Khare, A. Jentys, T. Huthwelker, C. N. Borca, A. Kalinko, O. Y. Gutiérrez, N. Govind, J. L. Fulton, J. Z. Hu, V.-A. Glezakou, R. Rousseau, M. Sanchez-Sanchez, J. A. Lercher, *JACS Au.* **2021**, *1*, 1412–1421.

Manuscript received: April 17, 2023
Revised manuscript received: April 18, 2023
Accepted manuscript online: April 19, 2023
Version of record online: ■■, ■■

RESEARCH ARTICLE

Protocol matters! This work shows how different ion exchange protocols impact SCR activity of Cu-SSZ-13, even when they lead to the same metal content. This work suggests an underappreciated approach to influencing catalytic activity.

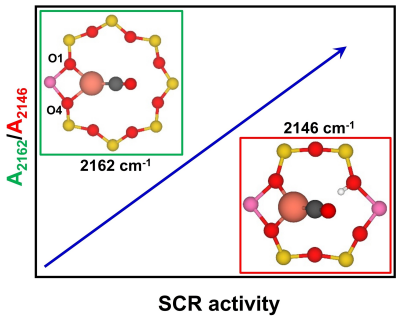

*Dr. A. Koishybay, Mr. C. Umhey, Dr. C.-T. Kuo, Mr. K. Groden, Prof. Dr. J.-S. McEwen, Prof. Dr. A. M. Karim, Prof. Dr. D. F. Shantz**

1 – 11

Elucidating the Effect of Ion Exchange Protocol on the Copper Exchange Efficacy, Copper Siting, and SCR activity in Cu-SSZ-13